





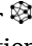





Functionalized aluminum-graphene oxide for enhanced ion transport in solid polymer electrolytes

Krystalynn Gracella Angeline ^a, Ridho Hantoro ^a, Nova Sartika Wulansari ^a, Fredina Destyorini ^b, Andri Hardiansyah ^c, Sylvia Ayu Pradanawati ^d, Lizda Johar Mawarani ^a, Nur Laila Hamidah ^{a*}

a : Departement of Engineering Physics, Institut Teknologi Sepuluh Nopember , Surabaya 60111, Indonesia

b : Research Center for Advanced Materials, National Research and Innovation Agency (BRIN) , Tangerang Selatan 15314, Indonesia

c : Research Center for Nanotechnology Systems, National Research and Innovation Agency (BRIN) , Tangerang Selatan, 15314, Indonesia

d : Departement of Mechanical Engineering, University of Pertamina, Jakarta 12220, Indonesia

* Corresponding author: nurlaila@its.ac.id

Abstract

This study reports the fabrication and characterization of aluminum-functionalized graphene oxide (GO-Al) composite membranes for solid polymer electrolyte applications. The aim of this work is to investigate how aluminum functionalization modifies the interlayer structure of graphene oxide membranes and influences ion transport behavior. Graphene oxide was synthesized via the Tour method and functionalized with Al³⁺ ions derived from AlCl₃ at different loadings of 3.52, 14.68, and 25.93 wt%. Intercalation of trivalent aluminum ions induced an expansion of the GO interlayer spacing from 0.8125 to 0.8278 nm and promoted the conversion of epoxy (C–O–C) groups into hydroxyl (C–OH) and carboxyl (C–OOH) groups through the formation of stable Al–O–C coordination bonds. These structural modifications enhanced membrane hydrophilicity, structural stability, and ion transport capability. Raman spectroscopy revealed increased structural disorder, while thermogravimetric analysis indicated improved thermal stability with reduced total weight loss. Electrochemical impedance spectroscopy demonstrated a significant enhancement in ionic conductivity from 0.282 to 0.553 S·m⁻¹, attributed to Grotthuss-type ion hopping through hydrated transport pathways. Among the investigated compositions, the GO–Al 25.93% membrane exhibited the most favorable balance between interlayer expansion, defect structure, and ionic transport performance, highlighting its potential as a solid polymer electrolyte.

Key findings

- Aluminum functionalization expanded the GO interlayer spacing and formed stable Al–O–C coordination bonds, resulting in enhanced structural integrity and hydrophilicity.
- Thermal stability was significantly improved, with total weight loss decreasing from 70.05% for pristine GO to 56.33% for the GO–Al 25.93% membrane.
- Ionic conductivity increased from 0.282 to 0.553 S·m⁻¹, which is attributed to Grotthuss-type ion hopping through hydrated transport channels.

© 2026, the Authors. This article is published in open access under the terms and conditions of the Creative Commons Attribution (CC BY) license (<http://creativecommons.org/licenses/by/4.0/>), which permits unrestricted reuse of the work in any medium provided the original work is properly cited.

Accompanying information

Article history

Received: 05.11.25

Revised: 03.01.26

Accepted: 12.01.26

Available online: 20.01.26

Keywords

aluminum;
graphene oxide;
ionic conductivity;
ion transport mechanism;
solid polymer electrolyte

Funding

This work was supported by Institut Teknologi Sepuluh Nopember Surabaya (ITS), Indonesia, through the scientific Research Grant (Contract No. 1728/PKS/ITS/2025).

Supplementary information

Transparent peer review: 

Sustainable Development Goals



1. Introduction

The extensive use of fossil fuels for power generation has caused significant environmental damage, and due to their non-renewable nature, the development of sustainable energy sources has become increasingly urgent [1]. Renewable energy sources such as wind, nuclear, and solar energy were developed in response to environmental concerns and the depletion of fossil fuel reserves [2]. Despite their advantages, these energy sources are inherently intermittent and cannot provide a continuous power supply. Consequently, substantial research efforts have focused on developing energy storage systems to address this intermittency. Among various options, batteries represent an effective solution, as they store chemical energy and convert it into electrical energy when required [3].

Traditional rechargeable batteries, including nickel–cadmium, lead–acid, and nickel–metal hydride batteries, commonly employ aqueous electrolytes [4]. However, these systems generally exhibit low energy density and relatively high weight. The development of lithium-ion batteries in the 1980s, followed by their commercialization in 1991, marked a major advancement in energy storage technology [5]. Lithium-ion batteries offer advantages such as low redox potential and small ionic radius [6]. Nevertheless, modern lithium-ion batteries remain limited in terms of long cycle life and high energy performance for portable electronics and electric vehicles [7]. Safety concerns related to liquid electrolytes have emerged due to several reported failure incidents [8]. The development of safer electrolytes with high thermal and chemical stability, along with strong ionic conductivity, is crucial for next-generation lithium battery technologies.

Solid polymer electrolytes (SPE) present a promising alternative owing to their solid-state nature, which enhances battery safety and enables efficient lithium-ion transport [9]. Numerous studies have investigated polymers such as poly(ethylene oxide) (PEO), poly(vinyl alcohol) (PVA), and poly(vinylidene fluoride) (PVDF) as SPE materials. PEO exhibits excellent ion solvation capability but suffers from high crystallinity at room temperature, which limits ion mobility [10]. PVA offers good mechanical properties but strong hydrogen bonding restricts ionic conductivity [11]. PVDF provides superior electrochemical stability, yet its rigidity reduces polymer chain mobility [12].

Graphene oxide (GO) has emerged as a promising solid-state electrolyte matrix due to its unique two-dimensional layered structure and large surface area. GO contains abundant oxygen-containing functional groups, such as hydroxyl, epoxy, and carboxyl groups [13]. These functional moieties enable ion coordination and migration through interlayer channels providing continuous ionic pathways within the lamellar framework [14]. The coexistence of sp^2 carbon domains and oxygenated sites provides both mechanical integrity and ionic functionality, supporting stable ion transport under solid-state conditions [14]. Recent studies have

demonstrated that tailored modification of GO can significantly improve functional performance, including enhanced ionic transport, increased surface charge density, and tunable defect structures, resulting in improved conductivity [15].

Structural optimization of GO has also been shown to enhance mechanical and electrical properties, including improved mechanical stability and more efficient ionic pathways relevant to energy storage and electrolyte applications [16]. Interlayer spacing is a critical structural parameter in GO that can be tuned through chemical modification or intercalation, enabling precise control of ion mobility and charge transfer across the layered framework [17,18]. Numerous studies have reported that functionalized GO derivatives exhibit enhanced ionic conductivity and improved stability, attributed to the formation of efficient ion-conducting networks and strengthened coordination environments compared to unmodified GO [19,20]. These improvements are often accompanied by enhanced mechanical strength, reduced swelling behavior, and improved thermal stability, which are essential for reliable performance in solid electrolyte applications [21].

Despite its excellent ionic transport capability and mechanical strength, the practical application of GO as a solid-state electrolyte remains limited by intrinsic instability. Oxygen-containing functional groups in GO are thermally and chemically labile, leading to partial degradation and deoxygenation at elevated temperatures [22]. This degradation weakens intersheet interactions and compromises the structural integrity of GO membranes [23]. The strong hydrophilicity of GO can cause excessive swelling and exfoliation under humid conditions, negatively affecting long-term stability [17].

Crosslinking has been developed as an effective strategy to reinforce the GO structure and stabilize functional groups through coordination bonding between adjacent layers. The incorporation of multivalent metal cations, including Na^+ , Ca^{2+} , Mg^{2+} , Fe^{3+} , and Al^{3+} , has been reported to improve the water stability, ion selectivity, and mechanical strength of GO membranes [24]. These multivalent cations interact with GO sheets via coordination with oxygen functional groups, electrostatic attraction to negatively charged sites, and cation– π interactions with sp^2 -conjugated carbon domains [25]. Such crosslinking enhances the chemical and thermal resistance of GO, thereby preventing structural degradation during membrane operation.

Aluminum-containing metal oxide–graphene composites have been reported to exhibit improved charge transport characteristics, structural robustness, and interfacial conductivity due to synergistic interactions between metal oxide active sites and the conductive graphene framework [25,26]. Structural modification and metal-assisted functionalization of graphene oxide-based materials can markedly enhance stability and charge transport behavior. The integration of metal or metal-oxide components into graphene-based

frameworks has been reported to improve interfacial conductivity, suppress structural degradation, and enhance electrochemical durability through strengthened interlayer interactions and defect regulation [27]. Aluminum-containing graphene composites exhibit improved charge transport pathways and structural robustness due to synergistic interactions between metal-derived active sites and the conductive graphene network.

Robertson et al. reported the modification of graphene oxide sheets by introducing Al^{3+} ions from Al_2O_3 , AlCl_3 , or aluminum foil into acidic GO suspensions prior to membrane self-assembly [28]. Al_2O_3 does not readily react with water to release Al^{3+} ions, and residual alumina particles can disrupt the lamellar structure, thereby reducing membrane stability. In contrast, AlCl_3 readily hydrolyzes in aqueous environments to generate Al^{3+} ions, which promote effective crosslinking between GO sheets and enhance mechanical stability in aqueous conditions. Accordingly, AlCl_3 was selected as the multivalent metal source in this study.

Therefore, this study aims to investigate the effect of aluminum functionalization on the interlayer structure of graphene oxide membranes and to elucidate the relationship between structural modification and ion transport behavior. The ionic conductivity of GO–Al composite membranes is systematically evaluated to identify the optimal aluminum content for solid polymer electrolyte applications.

2. Material and Methods

2.1. Materials

For the fabrication of graphene oxide (GO), expanded graphite (99%, Ito Graphite Co., Ltd., Japan), potassium permanganate (KMnO_4), sulfuric acid (H_2SO_4 , 98%), phosphoric acid (H_3PO_4 , 85%), hydrogen peroxide (H_2O_2 , 30%), hydrochloric acid (HCl , 37%), and distilled water were used. Aluminum chloride (AlCl_3 , Merck) was used as the source of Al^{3+} ions. All chemicals were of analytical grade and were used without further purification.

The equipment employed for membrane preparation included an oil bath, magnetic stirrer, centrifuge, ultrasonicator, vacuum filtration apparatus, and membrane filters with pore sizes of 0.4 μm and 180 μm .

2.2. Synthesis of Graphene Oxide

Graphene oxide was synthesized using a modified Tour method, as illustrated in Figure 1 and described in a previous study [26]. Briefly, 3 g of expanded graphite was mixed with 18 g of KMnO_4 , followed by the gradual addition of 360 mL of H_2SO_4 and 40 mL of H_3PO_4 . The mixture was stirred at 50 °C for 12 h to promote oxidation.

After cooling to room temperature, the reaction mixture was poured onto 400 mL of ice containing 6 mL of H_2O_2 until a bright yellow color appeared, indicating complete oxidation. The resulting suspension was washed three times with distilled water by centrifugation at 4000 rpm for 20–30 min until

neutral pH was achieved. The final product was ultrasonicated for 5 h to obtain well-exfoliated graphene oxide (GO) sheets.

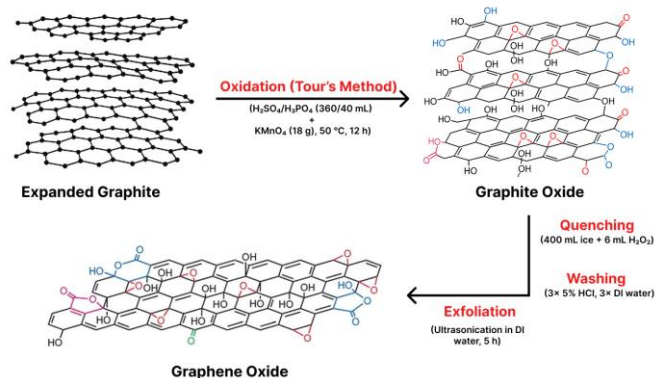


Figure 1 Schematic illustration of the synthesis of graphene oxide via the Tour's method.

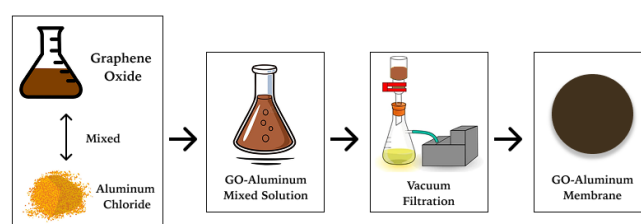


Figure 2 Schematic illustration of the preparation of the GO–Aluminum composite membrane.

2.3. Fabrication of GO–Aluminum Membrane

GO–Al composite membranes were prepared by incorporating Al^{3+} cations at different loadings of 3.52 wt% (GO–Al 3.52%), 14.68 wt% (GO–Al 14.68%), and 25.93 wt% (GO–Al 25.93%). For GO–Al 3.52%, 9.9 mg of GO was mixed with 0.36 mg of AlCl_3 . For GO–Al 14.68% and GO–Al 25.93%, 6.7 mg of GO was mixed with 1.16 mg and 2.36 mg of AlCl_3 , respectively. A schematic illustration of the GO–Al composite membrane preparation process is presented in Figure 2.

Each mixture was ultrasonicated to ensure homogeneous dispersion and then poured onto a stacked membrane filtration system consisting of 180 μm and 0.4 μm filters. Vacuum filtration was carried out at room temperature under atmospheric pressure, and the resulting membranes were dried under ambient conditions prior to characterization.

2.4. Characterization of GO–Aluminum Membrane

Various analytical techniques were employed to characterize the structural, thermal, and electrochemical properties of the GO and GO–Al composite membranes. X-ray diffraction (XRD, PANalytical X'Pert PRO) was used to analyze the crystal structure and interlayer spacing over a 2θ range of 0°–90°. Thermogravimetric analysis (TGA, Mettler Toledo TGA/DSC) was performed under an inert atmosphere from 0 to 600 °C to evaluate thermal stability and decomposition behavior. Structural disorder and defect density were analyzed using Raman spectroscopy (Horiba LabRAM HR Evolution) with a 532 nm excitation laser over a Raman shift

range of 0 – 3000 cm^{-1} . Fourier-transform infrared spectroscopy (FTIR, Thermo Scientific Nicolet iS10) was used to identify functional groups in the range of 1000–4000 cm^{-1} . Ionic conductivity and charge transfer resistance were measured using electrochemical impedance spectroscopy (EIS, Corrtest CS350 Potentiostat/Galvanostat) with a low-amplitude AC signal at room temperature (~ 300 K) over a frequency range of 0.1–100,000 Hz.

3. Result and Discussion

3.1. Graphene Oxide Interlayer

Figure 3 presents the X-ray diffraction (XRD) patterns of graphene oxide (GO) and aluminum-functionalized graphene oxide (GO-Al) composite membranes. The pristine GO sample exhibits a distinct diffraction peak at $2\theta = 10.88^\circ$, corresponding to the (001) reflection plane, which is characteristic of oxidized graphene oxide [29]. This peak represents the regular stacking of oxidized graphene layers. The interlayer spacing (d) was calculated using Bragg's law, expressed as follows:

$$n\lambda = 2d \sin \theta \quad (1)$$

where n is the diffraction order, λ is the X-ray wavelength, d is the interplanar spacing, and θ is the Bragg diffraction angle.

The calculated d -spacing value of 0.8125 nm for pristine GO is consistent with previous reports [30] and is attributed to the presence of oxygen-containing functional groups, such as hydroxyl ($-\text{OH}$), carboxyl ($-\text{COOH}$), and epoxy ($\text{C}-\text{O}-\text{C}$) groups. These functional groups expand the interlayer distance relative to pristine graphite, indicating successful oxidation and exfoliation of graphite into graphene oxide sheets.

Following aluminum functionalization, the (001) diffraction peak systematically shifted toward lower diffraction angles, with the corresponding peak positions and calculated interlayer spacings summarized in Table 1. The 2θ values for GO-Al 3.52%, GO-Al 14.68%, and GO-Al 25.93% were observed at 10.81° , 10.70° , and 10.68° , respectively. Correspondingly, the calculated interlayer spacing increased progressively from 0.8181 nm (pristine GO) to 0.8278 nm, representing interlayer expansions of approximately 0.68%, 1.73%, and 1.88%. The shift of the diffraction peak toward lower angles indicates an increase in interlayer spacing due to the intercalation of trivalent aluminum ions between adjacent GO sheets.

These XRD features indicate aluminum-induced structural rearrangement within the graphene oxide framework. In aluminum-functionalized GO membranes, similar XRD features have been reported to correlate with distinct morphological characteristics observed by SEM, including enlarged lamellar spacing, wrinkled sheet morphology, and improved layer organization [31]. SEM-EDS analyses in related GO-metal systems have demonstrated a homogeneous distribution of multivalent cations throughout the graphene

oxide matrix, supporting the interpretation that interlayer expansion detected by XRD originates from metal intercalation rather than simple physical adsorption [32].

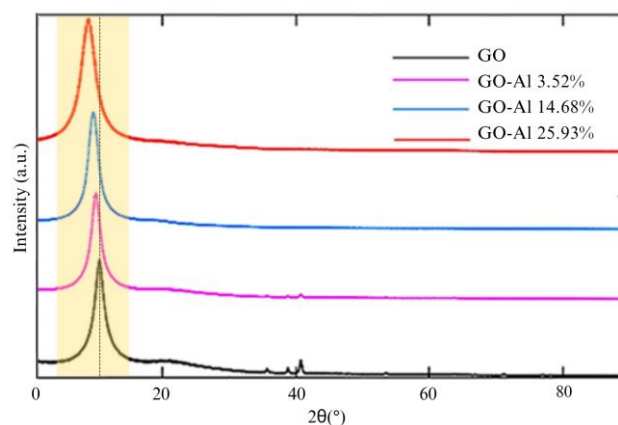


Figure 3 XRD patterns of GO and GO-Al composite membranes.

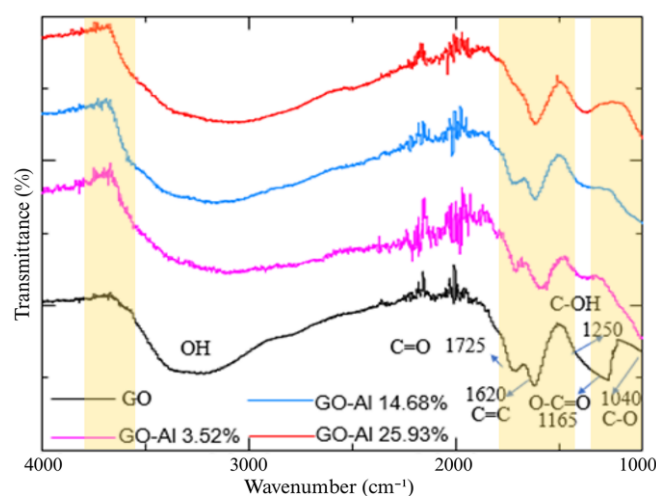


Figure 4 FTIR spectra of GO and GO-Al composite membranes.

Table 1 XRD peak position, interlayer spacing, and spacing expansion of GO and GO-Al samples.

Sample	2θ ($^\circ$)	d-Spacing (nm)	d-Spacing Expansion (%)
GO	10.88	0.8125	0
GO-Al 3.52%	10.81	0.8181	0.68
GO-Al 14.68%	10.70	0.8266	1.73
GO-Al 25.93%	10.68	0.8278	1.88

Accordingly, the present XRD results are consistent with previously reported SEM-EDS observations for metal-crosslinked graphene oxide systems, indicating aluminum incorporation and structural modification in the GO membranes.

Al^{3+} ions, acting as Lewis acids, strongly interact with oxygen-containing functional groups on the GO basal planes, particularly hydroxyl ($\text{C}-\text{OH}$) and epoxy ($\text{C}-\text{O}-\text{C}$) groups, leading to the formation of $\text{Al}-\text{O}-\text{C}$ coordination bonds. This coordination interaction partially disrupts the van der Waals-driven stacking of GO sheets, resulting in expanded interlayer galleries. The increase in interlayer spacing weakens the $\pi-\pi$ interactions between adjacent GO layers by introducing new ionic and coordination interactions

with surface oxygen functionalities. These structural modifications enhance the polarity and hydrophilicity of the GO layers, enabling the interlamellar galleries to accommodate hydrated cations and facilitating ion transport through the membrane. FTIR analysis further confirms that Al^{3+} coordination induces partial conversion of epoxy groups into hydroxyl groups, contributing to increased structural flexibility and improved bidirectional cation mobility.

Moreover, the broadening and reduced intensity of the diffraction peaks observed in GO-Al composites, compared to pristine GO, indicate a decrease in long-range crystalline order and an increase in structural disorder induced by aluminum intercalation. This disruption of periodic stacking is associated with partial exfoliation of GO sheets and non-uniform aluminum coordination on the basal planes. Although crystallinity is reduced, the presence of defect-rich regions provides additional pathways for rapid ion transport, thereby enhancing the ionic conductivity of the composite membranes.

3.2. Functional Group Analysis

Fourier transform infrared (FTIR) spectroscopy was employed to investigate the evolution of functional groups in GO and GO-Al composite membranes, as illustrated in Figure 5. The FTIR spectrum of pristine GO exhibits several characteristic absorption bands associated with oxygen-containing functional groups, confirming the successful oxidation of graphite. The broad and intense band observed in the $3000\text{--}3700\text{ cm}^{-1}$ region corresponds to O-H stretching vibrations arising from both intercalated water molecules and surface hydroxyl groups. The characteristic absorption peak at 1725 cm^{-1} is attributed to the stretching vibration of carbonyl (C=O) groups in carboxylic acid and carbonyl moieties, while the shoulder at approximately 1620 cm^{-1} is associated with C=C stretching within sp^2 -hybridized carbon domains. Additional absorption bands at 1165 cm^{-1} and 1040 cm^{-1} are characteristic of oxidized graphene structures and are assigned to carboxyl (O-C=O) and epoxy (C-O-C) groups, respectively.

Upon aluminum functionalization, noticeable changes in the FTIR spectra were observed. The intensities of hydroxyl and carboxyl-related absorption bands increased for the GO-Al 3.52%, GO-Al 14.68%, and GO-Al 25.93% membranes, while the epoxy (C-O-C) peak at approximately 1040 cm^{-1} gradually decreased. In addition, a new shoulder band appeared around 1250 cm^{-1} , which is attributed to the stretching vibration of C-OH groups in alkoxide species. These spectral changes indicate that Al^{3+} coordination induces partial transformation of epoxy functional groups into hydroxyl (C-OH) and carboxyl (C-OOH) groups.

Aluminum ions, acting as Lewis acids, preferentially coordinate with oxygen atoms in hydroxyl and carboxyl groups, forming Al-O-C and Al-O-H bonds. This coordination increases the polarity of the functional groups and enhances the hydrophilicity of the GO surface. The strengthened O-H and C-O bonds promote hydrogen bonding and

improve water retention within the membrane. Since water molecules serve as the transport medium for hydrated cations, these structural modifications facilitate ionic diffusion and enhance ionic conductivity in the composite membranes. The observed decrease in epoxy-related absorption is consistent with previous XPS studies [33], which reported a reduction in C-O-C functionalities accompanied by an increase in hydroxyl and carboxyl groups upon aluminum incorporation. Overall, these structural changes contribute to a more robust GO-Al framework with an increased density of ionically active sites.

3.3. Structural Disorder and Defect Analysis

Raman spectroscopy was employed to analyze the structural disorder, defect density, and layer characteristics of GO and GO-Al composite membranes, as shown in Figure 6. The Raman spectra of all samples exhibit two prominent peaks, such as the D band at approximately 1350 cm^{-1} and the G band at around 1580 cm^{-1} . The D band originates from the breathing mode of sp^2 carbon rings and is associated with structural defects and disorder in the graphene lattice. In contrast, the G band arises from the in-plane stretching vibration of sp^2 -hybridized carbon-carbon (C=C) bonds within graphitic domains. A less intense feature observed at approximately 2700 cm^{-1} corresponds to the 2D band, which provides information on the number of graphene layers and their stacking order.

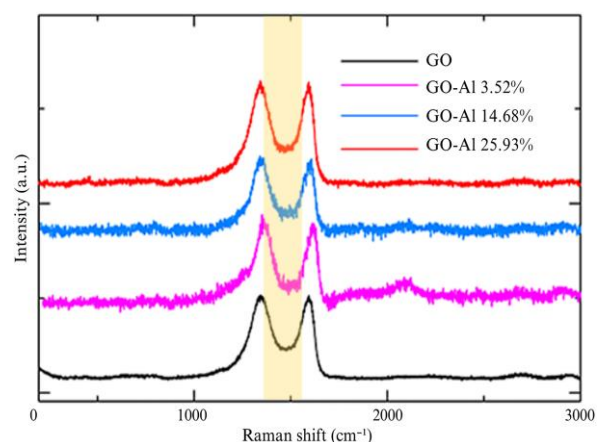


Figure 5 Raman spectra of GO and GO-Al composite membranes.

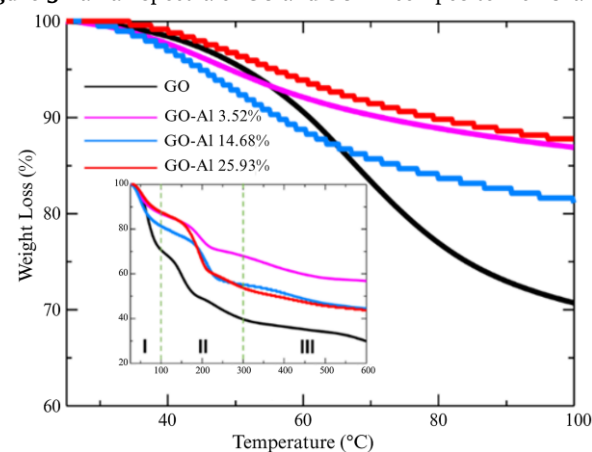


Figure 6 Thermogravimetric analysis (TGA) curves of GO and GO-Al composite membranes.

Table 2 Raman band positions and intensity ratios of GO and GO–Al composite membranes.

Sample Type	D-band (cm ⁻¹)	G-band (cm ⁻¹)	2D-band (cm ⁻¹)	I _D /I _G	I _G /I _{2D}
GO	1353.39	1585.472	2691.27	0.976	1.834
GO–Al 3.52%	1330	1594.962	2096.8	0.912	2.841
GO–Al 14.68%	1342.85	1369.876	2124.63	0.959	2.7
GO–Al 25.93%	1363.54	1513.568	2110.46	0.985	1.719

The positions and intensity ratios of the characteristic Raman bands are summarized in Table 2. Pristine GO exhibits D-, G-, and 2D-band positions at 1353.4, 1585.5, and 2691.3 cm⁻¹, respectively, with an I_D/I_G ratio of 0.976, indicating a moderate degree of structural disorder typical of oxidized graphene. Upon aluminum functionalization, slight shifts in the D- and G-band positions were observed, accompanied by changes in the I_D/I_G ratio. The I_D/I_G values for GO–Al 3.52%, GO–Al 14.68%, and GO–Al 25.93% were 0.912, 0.959, and 0.985, respectively. The gradual increase in the I_D/I_G ratio suggests a modest increase in defect density with increasing aluminum content.

The coordination of aluminum ions with oxygen-containing functional groups partially disrupts the sp² conjugated network of the GO lattice, leading to the formation of additional defect sites. The presence of Al–O–C and Al–O–H linkages, as confirmed by FTIR analysis, introduces localized strain and vacancy-type defects that increase the density of active sites for ion adsorption and transport. The moderate increase in the I_D/I_G ratio observed for the GO–Al 25.93% sample indicates an optimal balance between defect generation and preservation of graphitic domains, which is beneficial for maintaining electronic continuity while enhancing ionic accessibility.

The I_G/I_{2D} ratio provides further insight into the layer structure of the membranes. Pristine GO exhibits an I_G/I_{2D} value of 1.834, indicating a few-layer graphene structure. This ratio increased to 2.841 for GO–Al 3.52% and 2.700 for GO–Al 14.68%, suggesting the formation of thicker and more multi-layered structures due to aluminum-induced interlayer cross-linking. In contrast, the I_G/I_{2D} ratio decreased to 1.719 for the GO–Al 25.93% membrane, indicating partial exfoliation or improved dispersion of GO sheets. This observation is consistent with the XRD results showing increased interlayer spacing. The Raman analysis demonstrates that aluminum functionalization induces controlled structural disorder and modifies the stacking order of GO layers. The increased defect density facilitates ion transport by providing additional migration pathways, while the partial preservation of sp² domains ensures sufficient electronic connectivity within the membrane.

3.4. Thermal Stability

Thermogravimetric analysis (TGA) was employed to evaluate the thermal stability of GO and GO–Al composite membranes over a temperature range of 25–600 °C, as shown in

Figure 4. The TGA curve of pristine GO exhibits three distinct weight-loss regions, each corresponding to the removal of different structural components. The initial mass loss observed below 100 °C is attributed to the evaporation of physically adsorbed and interlayer water molecules. In this region, pristine GO exhibits a weight loss of 29.32%, reflecting its strong hydrophilicity and high content of oxygen-containing functional groups.

In contrast, the Al-functionalized GO composites exhibit lower mass losses in the same temperature range, with values of 13.10% for GO–Al 3.52%, 18.88% for GO–Al 14.68%, and 12.24% for GO–Al 25.93%. The reduced water loss indicates that aluminum functionalization strengthens the interactions between hydroxyl (–OH) groups and intercalated water molecules. These interactions decrease water volatility and suggest the formation of a more compact and cross-linked structure through Al–O coordination. The second decomposition region, occurring between 100 and 360 °C, corresponds to the removal of labile oxygen-containing functional groups and partial oxidative pyrolysis of the carbon framework. In this region, weight losses of 60.28% (GO), 32.04% (GO–Al 3.52%), 44.90% (GO–Al 14.68%), and 46.12% (GO–Al 25.93%) were observed. The significantly reduced mass loss in the GO–Al composites demonstrates that aluminum functionalization suppresses the thermal degradation of oxygenated moieties by forming thermally stable Al–O–C linkages.

The third decomposition stage, observed at temperatures above 360 °C, is associated with the oxidative combustion of the remaining carbon framework. In this region, the total weight losses were 70.05% for GO, 43.20% for GO–Al 3.52%, 55.46% for GO–Al 14.68%, and 56.33% for GO–Al 25.93%. Among the samples, the GO–Al 25.93% membrane exhibited the highest thermal resistance, as indicated by its higher residual mass and lower degradation rate. Aluminum functionalization enhances the thermal stability of GO membranes by strengthening interlayer bonding and preventing the decomposition of oxygen-containing functional groups. The formation of stable Al–O–C coordination networks contributes to improved structural robustness of the composite membranes at elevated temperatures.

3.5. Ionic Conductivity

Electrochemical impedance spectroscopy (EIS) was employed to evaluate the ionic conductivity behavior of GO and GO–Al composite membranes. The Nyquist plots presented in Figure 7 illustrate the impedance response of the samples along with the equivalent circuit model used for data fitting. The high-frequency intercept on the real axis represents the membrane resistance (R_m), while the semicircular region corresponds to the charge-transfer resistance (R_{ct}) at the electrode–electrolyte interface. The inclined line observed at lower frequencies is associated with the Warburg element (W_o), indicating ion diffusion through the membrane.

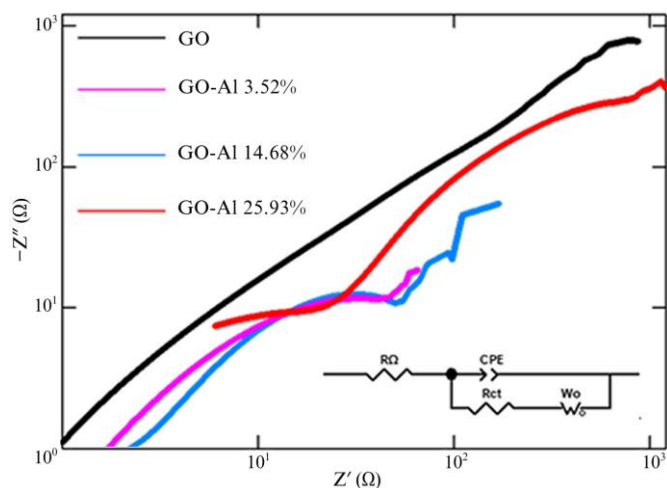


Figure 7 Nyquist plots of GO and GO-Al composite membrane.

The extracted electrical parameters revealed $R\Omega$ values of 223.7 Ω for GO, 280 Ω for GO-Al 3.52%, 300 Ω for GO-Al 14.68%, and 320 Ω for GO-Al 25.93%. The gradual increase in R_s with aluminum addition can be attributed to the denser membrane structure and enhanced interfacial bonding resulting from aluminum coordination. Despite the increase in bulk resistance, the presence of Al^{3+} ions enhances ionic transport by introducing additional hydrophilic and polar functional sites, which compensates for the higher R_s values.

Pristine GO exhibited a high charge-transfer resistance (R_{ct}) of $1.28 \times 10^6 \Omega$, indicating poor interfacial charge-transfer capability. Upon aluminum functionalization, the R_{ct} values decreased markedly to $5.26 \times 10^4 \Omega$ for GO-Al 3.52% and $6.27 \times 10^4 \Omega$ for GO-Al 14.68%, suggesting improved interfacial ion transport and an increased density of charge carriers. However, at the highest aluminum loading, the R_{ct} value increased significantly to $1.43 \times 10^6 \Omega$. This increase is likely associated with excessive aluminum incorporation, which may induce partial agglomeration or pore blockage, thereby restricting ion transport pathways.

The Warburg impedance (W_o), which reflects diffusion-controlled processes, exhibited negligible variation among

the GO-Al samples, indicating that ion diffusion is predominantly governed by the structural arrangement of GO layers rather than bulk diffusion limitations. The ionic conductivity (σ) was calculated using the following equation:

$$\sigma = \frac{L}{R_s A} \quad (2)$$

Here, L is the membrane thickness (cm), A is the electrode area (cm^2), and R_s is the membrane resistance (Ω).

The calculated ionic conductivity values were $0.282 S \cdot m^{-1}$ for GO, $0.287 S \cdot m^{-1}$ for GO-Al 3.52%, $0.397 S \cdot m^{-1}$ for GO-Al 14.68%, and $0.553 S \cdot m^{-1}$ for GO-Al 25.93%. These results demonstrate that aluminum functionalization significantly enhances the ionic conductivity of GO-based membranes. The improvement is attributed to the increased presence of hydrophilic and polar oxygen-containing functional groups (C-OH, C-OOH, and Al-O-C) introduced through Al^{3+} coordination, which facilitates ion hopping and water-assisted ionic conduction mechanisms.

3.6. Ion Transport Mechanism

The schematic illustration in Figure 8 compares the ion transport behavior in (A) pristine GO and (B) Al^{3+} -modified GO composite membranes. In pristine GO, the presence of abundant oxygen-containing functional groups, such as hydroxyl, carboxyl, and epoxy moieties, provides limited polar sites for cation transport. However, the relatively narrow interlayer spacing and the predominance of epoxy (C-O-C) linkages restrict the migration of hydrated ions through the membrane. As a result, ion transport primarily occurs via surface diffusion along the basal planes, leading to comparatively low ionic conductivity.

Upon aluminum functionalization, significant structural and chemical modifications occur within the GO framework. Al^{3+} ions coordinate with oxygen atoms in hydroxyl and carboxyl groups, promoting the conversion of epoxy (C-O-C) functionalities into alkoxide (C-OH) and carboxyl (C-OOH) species. This chemical transformation increases the density of hydrophilic sites and expands the interlayer spacing, thereby enhancing water molecule adsorption within the interlayer galleries.

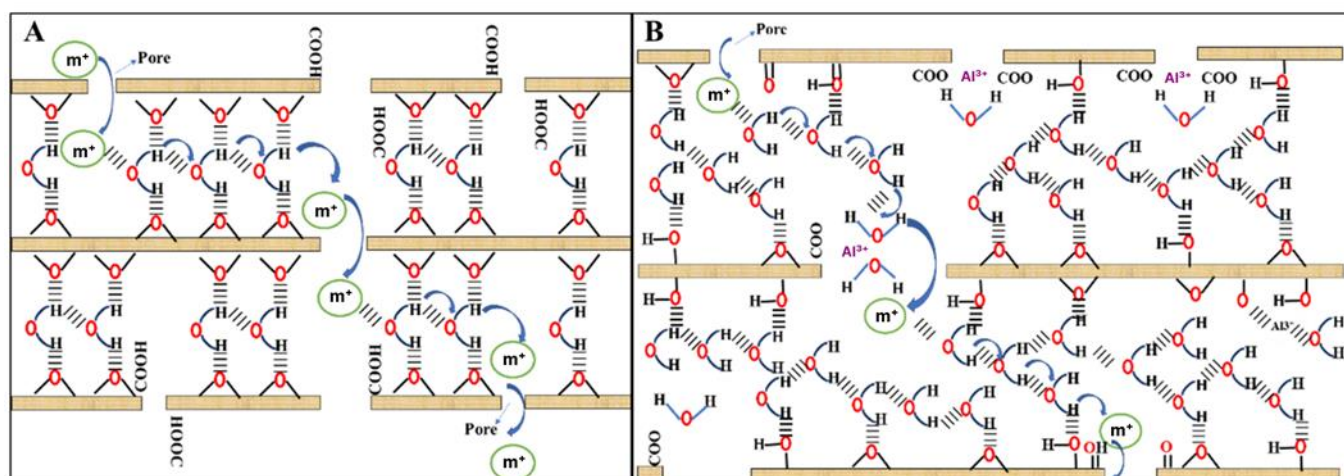


Figure 8 Schematic illustration of ion transport behavior in (A) pristine GO membrane and (B) Al^{3+} modified GO composite.

The increased presence of water molecules enables ion migration through a Grotthuss-type hopping mechanism, in which charge is transported via successive breaking and reforming of hydrogen bonds between adjacent water molecules [34]. The GO–Al 25.93% membrane exhibits a higher concentration of C–OH groups and larger interlayer spacing, resulting in more continuous and well-hydrated transport pathways. Consequently, ionic diffusion is significantly enhanced, leading to higher ionic conductivity compared to pristine GO.

This proposed mechanism is consistent with the EIS results, which show an increase in ionic conductivity from $0.282 \text{ S}\cdot\text{m}^{-1}$ for GO to $0.553 \text{ S}\cdot\text{m}^{-1}$ for the GO–Al 25.93% membrane. Coordinated Al^{3+} ions act as crosslinking centers that stabilize the GO layers while maintaining flexible and hydrophilic transport channels. The combined effects of interlayer expansion, chemical coordination, and hydrogen-bond-mediated ion hopping collectively contribute to the enhanced ionic mobility observed in the GO–Al composite membranes.

4. Limitations

This study has several experimental limitations that should be acknowledged. The use of aluminum chloride as the aluminum source may result in residual chloride species remaining within the GO–Al composite membranes, which could influence the long-term electrochemical stability and durability of the membranes. Although the GO–Al 25.93% membrane exhibited the most favorable performance, higher aluminum content may lead to non-uniform ion dispersion and partial agglomeration. Such effects could locally weaken the structural homogeneity of the membrane and influence its overall mechanical integrity. The electrochemical characterization in this study was conducted without repeated measurements; therefore, data repeatability and statistical variations, such as standard deviation values, were not evaluated. Consequently, the reported ionic conductivity values represent representative measurements under the applied experimental conditions.

5. Conclusions

This study demonstrates that aluminum functionalization effectively modifies the interlayer structure of graphene oxide membranes and enhances their ion transport behavior. The incorporation of Al^{3+} ions induces interlayer expansion and coordination with oxygen-containing functional groups, leading to increased hydrophilicity and structural rearrangement within the GO framework. Structural and thermal analyses confirm that aluminum coordination increases defect density while improving thermal stability, indicating successful crosslinking between adjacent GO sheets. Electrochemical impedance spectroscopy further reveals a significant enhancement in ionic conductivity,

which is attributed to aluminum-induced interlayer expansion and the formation of hydrated ion transport pathways governed by a Grotthuss-type hopping mechanism. Among the investigated compositions, the GO–Al 25.93% membrane exhibits the most favorable balance between structural modification and ion transport performance, highlighting its potential as a solid polymer electrolyte material for energy storage applications.

Acknowledgments

None.

Author contributions

Conceptualization: N.L.H., A.H., R.H.
 Data curation: N.S.W.
 Formal analysis: N.L.H., S.A.P.
 Funding acquisition: N.L.H., L.J.M.
 Investigation: K.G.A., N.S.W.
 Methodology: N.S.W., F.D., K.G.A.
 Project administration: R.H.
 Resources: R.H.
 Supervision: N.L.H., A.H., R.H.
 Validation: K.G.A., N.S.W.
 Visualization: K.G.A., N.S.W.
 Writing – original draft: K.G.A.
 Writing – review & editing: R.H., F.D., N.L.H., S.A.P.

Conflict of interest

The authors declare no conflict of interest

Additional information

Author IDs:

Krystalynn Gracella Angeline, Orc ID [0009-0003-6980-7443](https://orcid.org/0009-0003-6980-7443);
 Fredina Destyorini, Orc ID [0000-0001-8330-4429](https://orcid.org/0000-0001-8330-4429);
 Andri Hardiansyah, Orc ID [0000-0002-9505-3716](https://orcid.org/0000-0002-9505-3716);
 Ridho Hantoro Orc ID [0000-0001-6714-2933](https://orcid.org/0000-0001-6714-2933);
 Sylvia Ayu Pradanawati Orc ID [0000-0002-5520-6669](https://orcid.org/0000-0002-5520-6669);
 Nur Laila Hamidah, Orc ID [0000-0003-0777-4095](https://orcid.org/0000-0003-0777-4095);

Websites:

Institut Teknologi Sepuluh Nopember,
<https://www.its.ac.id/id/beranda/>
 National Research and Innovation Agency,
<https://www.brin.go.id/>
 Universitas Pertamina, <https://universitaspertamina.ac.id/>

References

1. Kenessova A, Seilkhanova G, Kurmanbayeva T, Ussipbekova E, Kurbatov A. Solid polymer electrolytes for energy storage systems. *Mater Today Proc.* 2020;31:588–91. doi:[10.1016/j.matpr.2020.07.106](https://doi.org/10.1016/j.matpr.2020.07.106)
2. Zhao H, Deng N, Yan J, Kang W, Ju J, Ruan Y, Wang X, Zhuang X, Li Q, Cheng B. A review on anode for lithium-sulfur batteries: Progress and prospects. *Chem Eng J.* 2018;347:343–65. doi:[10.1016/j.cej.2018.04.112](https://doi.org/10.1016/j.cej.2018.04.112)
3. Hu Q. Rechargeable Batteries for Renewable Energy: Current Status, Technical Challenges, and Future Directions. *E3S Web Conf.* 2025;606:02004. doi:[10.1051/e3sconf/202560602004](https://doi.org/10.1051/e3sconf/202560602004)
4. Mishra R, Malviya M, Tiwari P. Revolutionizing aqueous batteries: Exploring the challenges and thriving advancements. *J Energy Storage.* 2025;124:116787. doi:[10.1016/j.est.2025.116787](https://doi.org/10.1016/j.est.2025.116787)

5. Manthiram A, Yu X, Wang S. Lithium battery chemistries enabled by solid-state electrolytes. *Nat Rev Mater*. 2017;2(4):16103. doi:10.1038/natrevmats.2016.103
6. Wu X, Pan K, Jia M, Ren Y, He H, Zhang L, Zhang S. Electrolyte for lithium protection: From liquid to solid. *Green Energy Environ*. 2019;4(4):360–74. doi:10.1016/j.gee.2019.05.003
7. Chen H, Zheng M, Qian S, Ling HY, Wu Z, Liu X, Yan C, Zhang S. Functional additives for solid polymer electrolytes in flexible and high-energy-density solid-state lithium-ion batteries. *Carbon Energy*. 2021;3(6):929–56. doi:10.1002/cey2.146
8. Kiriyy N, Özenler S, Voigt P, Kobsch O, Meier-Haack J, Arnhold K, Janke A, Muza UL, Geisler M, Lederer A, Pospiech D, Kiriyy A, Voit B. Optimizing the Ion Conductivity and Mechanical Stability of Polymer Electrolyte Membranes Designed for Use in Lithium Ion Batteries: Combining Imidazolium-Containing Poly(ionic liquids) and Poly(propylene carbonate). *Int J Mol Sci*. 2024;25(3):1595. doi:10.3390/ijms25031595
9. Li S, Chen Y, Liang W, Shao Y, Liu K, Nikolov Z, Zhu Y. A Superionic Conductive, Electrochemically Stable Dual-Salt Polymer Electrolyte. *Joule*. 2018;2(9):1838–56. doi:10.1016/j.joule.2018.06.008
10. Li J, Zhu L, Xu J, Jing M, Yao S, Shen X, Li S, Tu F. Boosting the performance of poly(ethylene oxide)-based solid polymer electrolytes by blending with poly(vinylidene fluoride-co-hexafluoropropylene) for solid-state lithium-ion batteries. *Int J Energy Res*. 2020;44(9):7831–40. doi:10.1002/er.5476
11. Dennis JO, Shukur MF, Aldaghri OA, Ibnaouf KH, Adam AA, Usman F, Hassan YM, Alsadig A, Danbature WL, Abdulkadir BA. A Review of Current Trends on Polyvinyl Alcohol (PVA)-Based Solid Polymer Electrolytes. *Molecules*. 2023;28(4):1781. doi:10.3390/molecules28041781
12. Khan KH, Haleem A, Arwish S, Shah A, Hussain H. PVDF-based solid polymer electrolytes for lithium-ion batteries: strategies in composites, blends, dielectric engineering, and machine learning approaches. *RSC Adv*. 2025;15(26):20629–20656. doi:10.1039/D5RA02951A
13. Eslami B, Ghasemi I, Esfandeh M. Using Pegylated Graphene Oxide to Achieve High Performance Solid Polymer Electrolyte Based on Poly(ethylene oxide)/Polyvinyl Alcohol Blend (PEO/PVA). *Polymers*. 2023;15(14):3063. doi:10.3390/polym15143063
14. Fei W, Xue M, Qiu H, Guo W. Heterogeneous graphene oxide membrane for rectified ion transport. *Nanoscale*. 2019;11(3):1313–8. doi:10.1039/C8NR07557C
15. Murugan E, Poongan A, Dhamodharan A. Electrochemical sensing of acetaminophen, phenylephrine hydrochloride and cytosine in drugs and blood serum samples using β -AgVO₃/ZrO₂@g-C₃N₄ composite coated GC electrode. *J Mol Liq*. 2022;348:118447. doi:10.1016/j.molliq.2021.118447
16. Murugan E, Poongan A. A new sensitive electrochemical sensor based on BiVO₄/ZrO₂@graphene modified GCE for concurrent sensing of acetaminophen, phenylephrine hydrochloride and cytosine in medications and human serum samples. *Diam Relat Mater*. 2022;126:109117. doi:10.1016/j.diamond.2022.109117
17. Ma J, Ping D, Dong X. Recent Developments of Graphene Oxide-Based Membranes: A Review. *Membranes*. 2017;7(3):52. doi:10.3390/membranes7030052
18. Murugan E, Poongan A. Synchronous electrochemical detection of nanomolar acetaminophen, cytosine and phenylephrine hydrochloride in drugs using Zn₃V₂O₈/ZrO₂@f-MWCNTs nanocomposite GC electrode. *Results Chem*. 2023;5:100886. doi:10.1016/j.rechem.2023.100886
19. Murugan E, Poongan A. Electrochemical determination of caffeine in beverage using graphene oxide modified glassy carbon electrode. *Indian J Chem Technol*. 2021;28:528–36. doi:10.56042/ijct.v28i5.67603
20. Murugan E, Poongan A, Kesava M, Vinitha A. Synthesis and characterization of graphene nanosheets for electrochemical quantification of chlorpheniramine maleate drugs using a modified glassy carbon electrode. *Indian J Chem Technol*. 2022;29:713–20. doi:10.56042/ijct.v29i6.67423
21. Vinothkumar V, Poongan A, Mandal A, Venkatesh P. Electrochemical bio-sensor of caffeine in food beverages on using silver vanadium oxide decorated in graphitic carbon nitride (AgVO@g-CN) Nano composite modified glassy carbon electrode. *Sens Bio-sensing Res*. 2024;43:100637. doi:10.1016/j.sbsr.2024.100637
22. Cao L, Wu H, Yang P, He X, Li J, Li Y, Xu M, Qiu M, Jiang Z. Graphene Oxide-Based Solid Electrolytes with 3D Prepercolating Pathways for Efficient Proton Transport. *Adv Funct Mater*. 2018;28(50):1804944. doi:10.1002/adfm.201804944
23. Hu H, Gao T, Zhao X, Zhang J, Zhang Y, Qin G, Zhang X. Ultralight and high-elastic carbon foam with hollow framework for dynamically tunable electromagnetic interference shielding at gigahertz frequency. *Carbon*. 2019;153:330–6. doi:10.1016/j.carbon.2019.06.037
24. Li A, Han K, Zhou Y, Ye H, Liu G, Kung HH. Incorporating multivalent metal cations into graphene oxide: Towards highly-aqueous-stable free-standing membrane via vacuum filtration with polymeric filters. *Mater Today Commun*. 2017;11:139–46. doi:10.1016/j.mtcomm.2017.04.002
25. Liu T, Yang B, Graham N, Yu W, Sun K. Trivalent metal cation cross-linked graphene oxide membranes for NOM removal in water treatment. *J Membr Sci*. 2017;542:31–40. doi:10.1016/j.memsci.2017.07.061
26. Poongan A, Kesava M, Zeng H, Karthikeyan S, Jiang X. Development of a self-supported symmetric and asymmetric supercapacitor utilizing aluminum vanadium oxide microspheres enhanced with reduced graphene oxide (AIVO@RGO). *Inorg Chem Commun*. 2025;182:115663. doi:10.1016/j.inoche.2025.115663
27. Murugan A, Arumugam P, Vajiravelu S, Mandal A. Bio sensing of phenylephrine hydrochloride in medicinal samples using Carbon-based flexible 4d bimetallic ZnO nanocomposite coated Glassy Carbon Electrode. *J Mol Struct*. 2025;1321:139710. doi:10.1016/j.molstruc.2024.139710
28. Robertson EJ, Stehle YY, Hu X, Kilby L, Olsson K, Nguyen M, Cortez R. Al³⁺ Modification of Graphene Oxide Membranes: Effect of Al Source. *Membranes*. 2022;12(12):1237. doi:10.3390/membranes12121237
29. Athallah R, Pradanawati SA, Amanta RA, Pramata AD, Ayas N, Kida T, Hamidah NL. The Role of Graphene Oxide as a Filler and Lanthanum Nitrate as a Salt in Corn Starch-Based Solid Polymer Electrolytes. *Int J Technol*. 2025;16(2):512. doi:10.14716/ijtech.v16i2.7294
30. Wijanarko NP, Wulandari D, Helmi arrafii M, Ayu pradanawati S, Ni'Mah YL, Noerochim L, Laila hamidah N. Effect of Solid Polymer Electrolyte Based on Corn Starch and Lanthanum Nitrate on The Electrochemical Performance of Supercapacitor. *Bio Web Conf*. 2024;89:03001. doi:10.1051/bioconf/20248903001
31. Ahmad H, Liu C. Ultra-thin graphene oxide membrane deposited on highly porous anodized aluminum oxide surface for heavy metal ions preconcentration. *J Hazard Mater*. 2021;415:125661. doi:10.1016/j.jhazmat.2021.125661
32. Deng Z, Tang T, Huo J, He H, Dai K. Fabrication of Functionalized Graphene Oxide–Aluminum Hypophosphite Nanohybrids for Enhanced Fire Safety Performance in Polystyrene. *Polymers*. 2024;16(21):3083. doi:10.3390/polym16213083
33. Hamidah NL, Shintani M, Ahmad fauzi AS, Kitamura S, Mission EG, Hatakeyama K, Sasaki M, Quitain AT, Kida T. Electrochemical hydrogen production from humid air using cation-modified graphene oxide membranes. *Pure Appl Chem*. 2021;93(1):1–11. doi:10.1515/pac-2019-0807
34. Hamidah NL, Ahamd fauzi AS, Putri GK, Soegiantoro GH, Pratama PR, Darmawan A, Panatarani C, Prima EC, Xu W, Nidome T, Hatakeyama K, Quitain AT, Kida T. Self-Standing and Flexible Silk Fibroin-Modified Graphene Oxide Membrane for Selective Hydrogen Permeation. *ACS Appl Nano Mater*. 2025;8(43):21072–86. doi:10.1021/acsanm.5c04245